Single-photon absorption of isolated collagen mimetic peptides and triple-helix models in the VUV-X energy range

Schwob, Lucas; Lalande, Mathieu; Rangama, Jimmy; Egorov, Dmitrii; Hoekstra, Ronnie; Pandey, Rahul; Eden, Samuel; Schlathölter, Thomas; Vizcaino, Violaine; Poully, Jean-Christophe

Published in:
PPCP : Physical Chemistry Chemical Physics

DOI:
10.1039/c7cp02527k

Document Version
Final author's version (accepted by publisher, after peer review)

Publication date:
2017

Physical Chemistry Chemical Physics

ARTICLE

Single-photon absorption of isolated collagen mimetic peptides and triple-helix models in the VUV-X energy range

Received 00th January 20xx,
Accepted 00th January 20xx

DOI: 10.1039/x0xx00000x

www.rsc.org/

L. Schwob[a], M. Lalande[a], J. Rangama[a], D. Egorov[b], R. Hoekstra[b], R. Pandey[c], S. Eden[c], T. Schlathölter[b], V. Vizcaino[a] and J.–C. Poully[*a]

Cartilage and tendons owe their special mechanical properties to the fibrous collagen structure. These strong fibrils are aggregates of a sub-unit consisting of three collagen proteins wound around each other in a triple helix. Even though collagen is the most abundant protein in the human body, the response of this protein complex to ionizing radiation has never been studied. In this work, we probe the direct effects of VUV and soft X-ray photons on isolated models of the collagen triple helix, by coupling a tandem mass spectrometer to a synchrotron beamline. Single-photon absorption is found to induce electronic excitation, ionization and conversion into internal energy leading to inter- and intra-molecular fragmentation, mainly due to Gly-Pro peptide bond cleavages. Our results indicate that increasing the photon energy from 14 to 22 eV *reduces* fragmentation. We explain this surprising behavior by a smooth transition from excitation to ionization occurring with increasing photon energy. Moreover, our data support the assumption of a stabilization of the triple helix models by proline hydroxylation *via* intra-complex stereoelectronic effects, instead of the influence of solvent.

Introduction

One quarter of the human body protein content is collagen, the main constituent of skin, bone, cartilage and tendons. The latter owe their mechanical properties to the collagen fibrous structure. The strength of these fibrils is due to the aggregation of long fibers made of three proteins wound around each other in the characteristic collagen triple helix structure [1]. Many studies have been devoted to the triple helix stability and assembly in various solvents as well as to the design of collagen mimetic peptides [2,3]. In particular, the peptides $(PPG)_{10}$ and $(PHypG)_{10}$ are widely used triple helix models (P: proline, Hyp: hydroxyproline, G: glycine), with Hyp significantly increasing the thermal stability of the helix in solution [4,5]. UV irradiation of collagen and triple-helix models has been performed in solution, showing that the radicals created cause significant and specific cleavage of Gly-Pro peptide bonds, accompanied by transition from helical to random coil conformations [6–9]. However, to our knowledge the interaction of collagen mimetic peptides with ionizing radiation has not been studied in the gas-phase previously.

In this work, we probe the processes induced by ionizing photon irradiation of the isolated collagen mimetic peptides $(PPG)_{10}$ and $(PHypG)_{10}$ and their trimer triple helix models, by coupling a dedicated home-built tandem mass spectrometer [10] to VUV and soft X-ray beamlines of the BESSY-II synchrotron (Helmholtz Zentrum Berlin, Germany). The strength of our approach is the total control of the stoichiometry of the non-covalent complex of interest. This is crucial for collagen, because solely three strands give rise to the characteristic triple helix structure. Furthermore, the intrinsic response to irradiation can be probed without any influence of a solvent. Previous investigations on biologically-relevant molecular systems in the gas phase by means of VUV to soft X-ray synchrotron radiation have revealed that proteins, oligonucleotides and their building blocks (amino acids, peptides, nucleobases…) can be photoionized by single photon absorption *via* electron removal from valence (VUV) or atomic (X-ray) orbitals [11]. The accompanying electronic excitation can induce fragmentation if the molecular heat capacity is small enough that internal temperatures sufficient for thermal fragmentation are reached [12]. Reports on photoionization of non-covalent complexes of biomolecules are scarce [13–15], mainly focused on the binding site of a ligand to a protein, and have not yet covered the X-ray range. The present experiments study the effect of non-covalent binding between collagen mimetic peptides on the processes induced by photoabsorption over a wide energy range (14-288 eV). The role of proline hydroxylation is also investigated.

Experimental section

All experiments were performed at the BESSY-II synchrotron of the Helmholtz-Zentrum Berlin, by coupling a home-made tandem mass spectrometer to the U49/2-PGM1 beamline for soft X-ray photons (150 and 288 eV), or to the U152/2 NIM beamline for VUV photons (12-30 eV). The set-up is shown in figure 1 and has been described in detail elsewhere [16]. Briefly,

[a] *CIMAP, UMR 6252 (CEA/CNRS/ENSICAEN/Université de Caen Normandie), Caen, France*
[b] *Zernike Institute for Advanced Materials, University of Groningen, Nijenborgh 4, 9747AG Groningen, Netherlands*
[c] *Dept. of Physical Sciences, The Open University, Walton Hall, Milton Keynes, MK7 6AA, UK*
* *corresponding author: poully@ganil.fr*

protonated peptides and their non-covalent complexes were produced by means of electrospray ionization, mass-over-charge (m/z) selected by a Quadrupole Mass Spectrometer (QMS), and accumulated in a Paul trap where they were irradiated by the photon beam. The cations produced were analyzed by means of Time-Of-Flight (TOF) mass spectrometry.

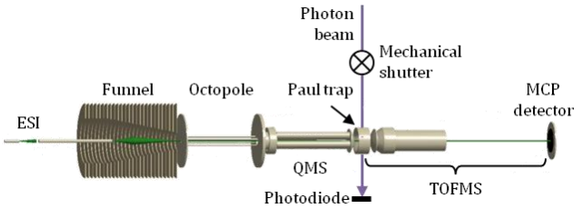

Figure 1 Sketch of the experimental set-up.

The collagen mimetic peptides $(PPG)_{10}$ and $(PHypG)_{10}$ have been purchased from Peptides International (> 95 % purity) and used without further purification. The powder has been dissolved in HPLC grade water/methanol (50:50 in volume; no acid added) at a concentration of around 100 µmol/L. A syringe pump drove the solution at a flow rate of 70 µL/mn. The electrospray needle was biased at 4 kV and located at a distance of 5 mm in front of a stainless-steel capillary (T ≈ 350 K; inner diameter: 0.76 mm; length: 20 cm) biased at 100 V. The ion beam emitted from the capillary was phase-space compressed by the combined radiofrequency (RF)+DC fields created by an ion funnel composed of 26 electrodes (DC voltage linearly decreasing from 25 to 13 V; RF = 276 kHz; V_{pp} = 170 V) at a pressure of 4.10^{-1} mbar. The ions were then collected in the next chamber at 5.10^{-4} mbar by an octopole (RF = 582 kHz; Vpp = 430 V), followed by an exit diaphragm with a bias voltage of 40 V. Then, the ions were extracted during 100 ms and m/z selected by a QMS (1.10^{-6} mbar) before being bunched into a commercial Paul trap (Jordan Inc.). Trapping was aided by a pulse of He buffer gas of similar duration. The QMS can also be operated in guiding mode (where only the RF is on), in order to monitor all ions within a broad m/z range. The synchrotron beam was sent through the trap orthogonally to the molecular ion axis and focused at the trap center to optimize the beam overlap. The irradiation time was set by controlling a mechanical shutter, and the relative photon flux was monitored by a SXUV-type silicon p–n junction photodiode (Opto Diode, Camarillo, US). Typical photon fluxes were $10^{12\text{-}13}$ s^{-1}, and the energy resolution was $\frac{E}{\Delta E} \approx 1000$. To keep the contribution of multiphoton absorption low, we tuned the irradiation time to ascertain a maximum of 10 % for the precursor ion depletion. The trapped cations were then extracted by a high voltage pulse applied to the hyperbolic electrodes, and accelerated by another set of electrodes, before being detected by microchannel plates (MCPs) biased at -5 kV. The signal was finally recorded by a 1 GHz digitizer (Teradyne, North Reading, US). The typical resolution of the TOF spectrometer was $\frac{TOF}{\Delta TOF} \approx 500$. The experimental period was 1 s, and we acquired one "photon beam off" spectrum (with the shutter closed) for two "photon beam on" spectra. Typically 500 of these cycles were necessary to obtain acceptable statistics, and we subtracted these "photon beam off" spectra from the "photon beam on" spectra. The result is a negative peak for the precursor ion and positive peaks for photoproduct ions. The resulting spectra were smoothed by adjacent averaging over 20 points, and calibrated in m/z. We also irradiated the trap residual gas without a molecular ion beam (by turning off the electrospray needle voltage) and recorded a spectrum for each photon energy (E_{ph}) to spot background peaks.

For E_{ph} below 14 eV, the beam is possibly contaminated by higher harmonics from the undulator, leading to contribution of photons of higher energy. Therefore, we could not rely on the intensity of peaks at lower energy than 14 eV, close to the threshold ionization energy of these species.

Since the detection efficiency of MCPs depends on ion velocity and thus m/z, all ion yields determined from the mass spectra were corrected by the detector efficiency, with the same method as reported earlier [11].

Results and Discussion

Source spectrum

To study collagen mimetic peptides in the gas phase, we dissolved the powder in a water/methanol solution and used an electrospray ionization source (see the experimental section). In aqueous solution, it is known from the literature that collagen mimetic peptides form trimers with a triple helix structure [4]. To reveal which species are produced in the electrospray process, a typical mass spectrum of electrosprayed ions from $(PPG)_{10}$ solution is shown in figure 2. The main peaks are doubly- and triply-protonated $(PPG)_{10}$ monomers (M^{2+} at m/z = 1266.4 and M^{3+} at 844.6). We cannot completely rule out the contribution of 6+ and 4+ dimers or 9+ and 6+ trimers. However, the additional peaks at slightly higher m/z, which can be assigned to H_2O adducts and Na^+ and K^+ ions substituting for one proton (see figure 4) indicate that monomers are the dominating contribution. At m/z = 1085.6, we observe unambiguously the protonated trimer $[((PPG)_{10})_3+7H]^{7+}$ noted T^{7+}. The observation of M^{2+} and M^{3+} is in line with the 7+ trimer charge state, if we assume that it is composed of one 3+ and two 2+ monomers. This is also the expected statistical distribution of protons. The relative peak intensities in the spectrum do not reflect the relative abundance of the species formed by ESI, since they also depend on the QMS and funnel settings. After the electrospray ionization source, the ions enter a radiofrequency ion funnel and undergo many residual gas collisions. Therefore, it is likely that most of the trimers separate into monomers due to collision-induced dissociation (CID). This process has been reported previously for multiply-protonated molecular complexes in the same low collision kinetic energy range [17–19].

Our spectrum is thus consistent with the $[((PPG)_{10})_3+7H]^{7+}$ trimer containing two $[(PPG)_{10}+2H]^{2+}$ and one $[(PPG)_{10}+3H]^{3+}$. It is important to note that we obtained a similar source spectrum for $(PHypG)_{10}$ (*cf.* figure S1), the other collagen mimetic peptides studied here. In addition to the T^{7+}, however, for $(PHypG)_{10}$ an additional peak that can be assigned to the five-fold protonated dimer is observed. This finding supports our assumption on the monomer charge state distribution within the peptide trimers.

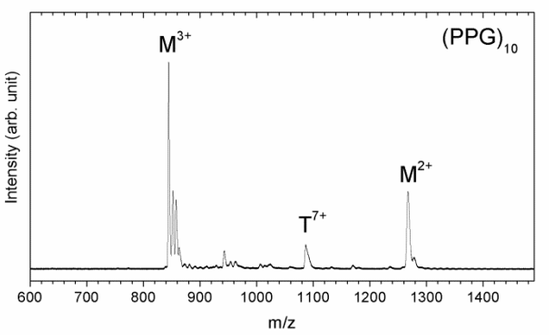

Figure 2 electrospray ionization source mass spectrum of a water/methanol solution of the $(PPG)_{10}$ collagen mimetic peptide.

Photoabsorption mass spectra of peptide monomers

The mass spectra of the isolated $[(PHypG)_{10}+3H]^{3+}$ peptide monomer after absorption of a single photon of 14, 22, 32 and 288 eV are shown in figure 3b. For comparison, the mass spectrum for $[(PHypG)_{10}+2H]^{2+}$ at 14 eV is plotted in figure 3c. The precursor ions (at m/z = 1266.4 for $[(PPG)_{10}+2H]^{2+}$ and m/z = 844.6 for $[(PPG)_{10}+3H]^{3+}$) are not visible because of the employed data analysis (see the experimental section). In all these spectra, we observe singly ionized intact peptide ions $[(PHypG)_{10}+2H]^{3+}$ and $[(PHypG)_{10}+3H]^{4+}$ at m/z = 844.3 and 633.4, respectively, due to non-dissociative ionization. We also observe fragments resulting predominantly from glycine-proline peptide backbone bond cleavages, giving series of singly-charged b_{3n} or doubly-charged b_{6n} (they have the same m/z) and y_{3n} fragments (n being a positive integer). In the high energy spectra, at 288eV, new fragment ions appear below m/z = 250. We attribute the main ones to internal fragments formed by at least two backbone cleavages (see figure 3a). This is in line with our previously reported mass spectra of peptides after X-ray single photon absorption: we showed that peptides of similar size or smaller undergo extensive fragmentation into low-mass ions due to one or two bond cleavages [12,20].

The relative intensity of the peaks due to the different relaxation pathways (non-dissociative ionization and backbone fragmentation) depends on photon energy E_{ph} but also on the initial charge state of the peptide. The most striking difference between the doubly- and triply protonated monomers is the significantly higher fragmentation yield for the latter. To gain deeper insight into the different processes triggered by single photon absorption, we have measured mass spectra for doubly- and triply-protonated monomers in the E_{ph} range 14-288eV for both $(PPG)_{10}$ and $(PHypG)_{10}$. Since the mass spectra contain peaks that can be assigned to the same species (except H_2O loss after ionization, see the next sub-section) and follow the same trend for both, we only present the experimental data for the hydroxylated peptide.

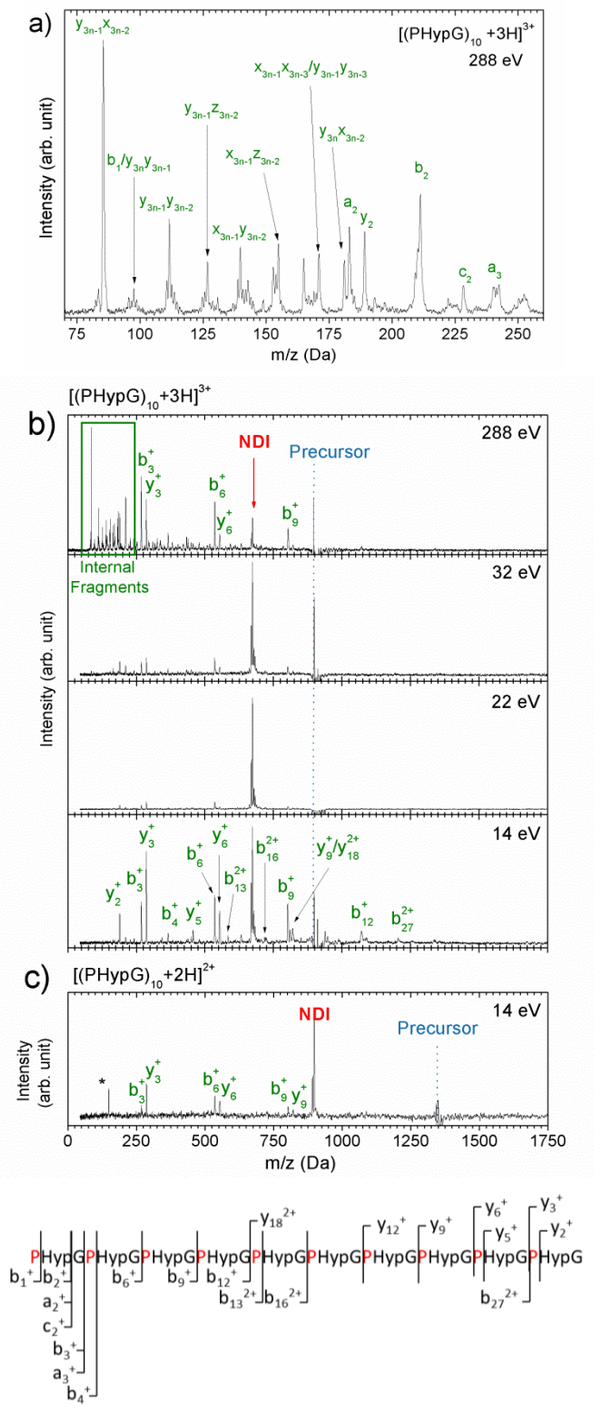

Figure 3 Photoabsorption mass spectra of $[(PPG)_{10}+3H]^{3+}$ at 14, 22, 32 and 288 eV (b) and of $[(PPG)_{10}+2H]^{2+}$ at 14 eV (c). The position of the precursor ion is indicated by dots, as the corresponding peak appears negative (see the experimental section). NDI stands for non-dissociative ionization, the main fragment ions have been assigned, and the asterisk spots a background peak. On panel a), we add a zoom into the m/z = 70-260

region of the mass spectrum of $[(PHypG)_{10}+3H]^{3+}$ at E_{ph} = 288eV. All fragment ions are singly-charged, and the nomenclature for internal fragments stands for the two bond cleavages needed for their formation. The peptidic sequence with the main cleavage sites and the fragments formed are shown in the bottom of the figure.

Non-dissociative ionization of peptide monomers

As shown in figure 3, non-dissociative ionization is already observed for E_{ph} = 14eV, giving the intact $[(PPG)_{10}+2H]^{3+}$ and $[(PPG)_{10}+3H]^{4+}$ peptide ions at m/z = 844.3 and 633.4. This is consistent with the reported experimental ionization energies of peptides of similar size and charge states (doubly protonated peptides: [Arg-8]-vasopressin: 11.7 ± 0.3 eV; substance P: 11.1 ± 0.6 eV; renin substrate: 12.2 ± 0.7 eV; triply protonated peptide: insulin B-chain: 13.3 ± 0.4 eV[21]).

Figure 4 shows a superimposition of the peaks corresponding to the precursor and intact ionized peptide ions. The additional features on the high mass side of the peaks are already observed in the in-source CID of $((PPG)_{10})_3$ (*cf.* figure 1). They can be assigned to non-covalent binding of H_2O and/or Na^+ and K^+ (substituting for one of the protons) to the isolated peptide. Both patterns are similar, showing that single photoionization mostly keeps these non-covalent complexes intact, even at 288 eV.

On the low mass side of the peak assigned to non-dissociative ionization, we observe the presence of an intense peak at m/z = 668.9 that can be attributed to H_2O loss. This loss is observed from doubly and triply protonated $(PHypG)_{10}$ and to a much weaker extent from $(PPG)_{10}$ (see figure S2). We have already observed similarly pronounced H_2O loss for a collagen hydroxylated peptide (the 423-448 amino-acid sequence of the α-1 chain of type I collagen), together with loss of other neutral molecules, and showed that they originate from side-chains [22]. Contrary to proline, the hydroxyproline side-chain contains an OH group, which is most probably involved in the pronounced H_2O loss. Interestingly, the relative intensity of this peak (about 50 % of non-dissociative ionization) does not depend on E_{ph} (*cf.* figure 4). Moreover, we do not observe such an intense peak corresponding to H_2O loss from the precursor. This is consistent with this process being due to ionization and occurring with a very low barrier, presumably a radical-driven rearrangement followed by H_2O loss, akin to the case of the 423-448 sequence of collagen [22].

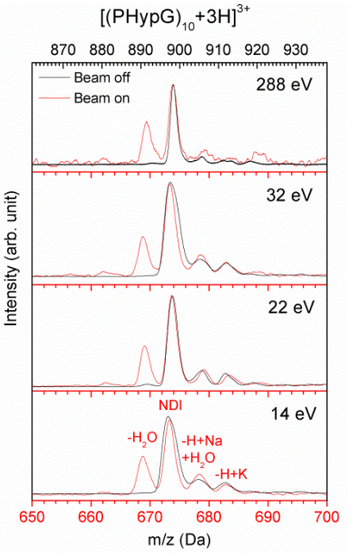

Figure 4 Superimposition of the mass spectra of $[(PHypG)_{10}+3H]^{3+}$ without (black line) and with (red line) photon beam after photoabsorption of one 14, 22, 32 and 288 eV photon. H_2O loss from the ionized peptide has been indicated, as well as Na^+ and K^+ substitutions for one proton.

Non-dissociative ionization and fragmentation *vs.* photon energy

To provide further insights into photoinduced processes in collagen mimetic peptides, figure 5a shows the relative yield of non-dissociative ionization and of the sum of all backbone fragment ions as a function of E_{ph}, for $[(PHypG)_{10}+2H]^{2+}$ and $[(PHypG)_{10}+3H]^{3+}$. This relative yield is defined as $RY = \frac{A}{A_p}$, where A and A_p are the absolute integrated area under the peak(s) of interest and the precursor ion depletion peak, respectively. Note that the areas are corrected by the detector efficiency, as stated in the experimental section. For both charge states, non-dissociative ionization first increases with photon energy from 14 to 20 eV and then decreases up to 288 eV. This trend has been observed over shorter energy ranges for photoionization of various neutral molecules [23] and singly-protonated substance P [24], as well as for electron impact ionization of multiply-protonated peptides [25]. There is a clear shift of the non-dissociative ionization yield with protonation state: for $[(PHypG)_{10}+3H]^{3+}$, it starts increasing at slightly higher E_{ph}. This result is consistent with studies by Giuliani *et al.* [26] and Budnik *et al.* [21] who showed that the ionization energy of a protonated peptide increases with its charge-state due to Coulomb interaction between the ejected electron and the molecular cation.

For both protonation states, the decrease in non-dissociative ionization above 20 eV is accompanied by an increasingly abundant fragmentation, which becomes the dominant channel between 30 and 40 eV (see figure 5, top panel). This is consistent with an increase of the peptide excitation energy with photon energy, as more and more strongly bound valence electrons become accessible for photoionization. Below 20 eV,

however, fragmentation increases with *decreasing* E_{ph} and becomes dominant at 14 eV for $[(PHypG)_{10}+3H]^{3+}$. These opposite trends for non-dissociative ionization and fragmentation indicate that in this energy range, fragmentation is not due to photoionization, but rather induced by photoexcitation of the peptides into highly excited electronic states, followed by internal conversion and intramolecular vibrational redistribution (IVR). This has been observed in photoabsorption of organic molecules over the same energy range [27]. Our data are thus consistent with neutral highly-excited states smoothly converging to the ground-state ionized species. Moreover, the fact that non-dissociative ionization (*cf.* figure 3) coexists with fragmentation over the entire present energy range shows that a single photon can probe a number of molecular valence orbitals. This is in agreement with photoelectron emission experiments on amino acids [28] and dipeptides [29]. Interestingly, the evolution of excitation *vs.* ionization is qualitatively similar to soft X-ray photoabsorption spectra obtained for gas-phase protonated proteins [30] at the C, N and O K-edges. Here again, photoexcitation and direct ionization show opposite trends with photon energy.

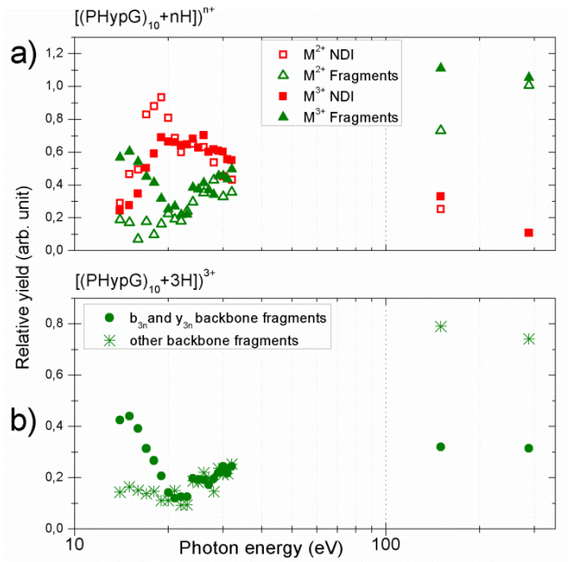

Figure 5 a) Relative yield of non-dissociative ionization (NDI) and of the sum of all backbone fragment ions observed as a function of E_{ph}, for $[(PHypG)_{10}+2H]^{2+}$ (M^{2+}) and $[(PHypG)_{10}+3H]^{3+}$ (M^{3+}). b) Relative yield of the sum of b_{3n} and y_{3n} fragments (*i.e.* b_{3n}^{+}, b_{3n}^{2+}, y_{3n}^{+} and y_{3n}^{2+}), and of the sum of other fragments, as a function of E_{ph}. All yields have been obtained by calculating the peak areas and normalizing by the precursor ion depletion.

Fragmentation of peptide monomers after photoabsorption

To shed light on the different processes underlying backbone fragmentation, it is useful to plot the relative yield of the sum of $\boldsymbol{b_{3n}^{+}}$, $\boldsymbol{b_{3n}^{2+}}$, $\boldsymbol{y_{3n}^{+}}$ and $\boldsymbol{y_{3n}^{2+}}$ fragments (presumably due to single backbone cleavage), as well as the sum of other backbone fragments (presumably due to multiple backbone cleavages), as a function of E_{ph} for $[(PHypG)_{10}+3H]^{3+}$ (see figure 5b). This shows that single and multiple backbone cleavage are dominant at low and high energy, respectively. Most single backbone cleavages occur N-terminal to proline residues. This preferential cleavage site (the so-called proline effect) has been observed previously in CID or UV photofragmentation of proline-containing peptides [31–33]. This is consistent with the fact that in our experiment, these fragments are mainly formed at low energy when photoexcitation without ionization dominates. We can infer that the higher fragmentation yield of $[(PHypG)_{10}+3H]^{3+}$ compared to $[(PHypG)_{10}+2H]^{2+}$ is mainly due to the additional proton, which can be transferred at a backbone N and induce bond cleavage. This "mobile proton" mechanism is widely known in CID of protonated peptides [34], and has been used to explain the proline effect [33,35,36]. The dominance of multiple backbone cleavages at high photon energy can be attributed to increasing internal energy transferred to the peptides after photoabsorption, leading to further dissociation of the fragments formed by single backbone bond cleavage.

Photoabsorption mass spectra of collagen triple helix model peptide trimers

To investigate the excitation and ionization processes within the $((PPG)_{10})_3$ and $((PHypG)_{10})_3$ collagen triple helix models in the gas phase, we studied photoabsorption for E_{ph} = 14-288 eV.

The $((PPG)_{10})_3$ peptide trimer

In figure 6a, we show mass spectra of the non-covalent complexes $[((PPG)_{10})_3]^{7+}$ after single photon absorption at E_{ph}= 14, 22, 30, 150 and 288 eV. The peak at m/z = 950.0 observed in all spectra corresponds to $[((PPG)_{10})_3+7H]^{8+}$, *i.e.* non-dissociative ionization of $[((PPG)_{10})_3+7H]^{7+}$. The observation of non-dissociative ionization at 14 eV is consistent with the ionization threshold energies of the 7+ charge state of cytochrome C and ubiquitin (reported to be lower than 14 eV [26]), two proteins similar to $((PPG)_{10})_3$ in size. Magnifications of the 14, 22 and 150 eV mass spectra are shown in figure 6b, where the non-dissociative ionization and precursor ion peaks are superimposed. We can clearly see peaks corresponding to several species: the trimer with seven protons, but also H_2O adducts, and Na^+/K^+ ions substituting for one proton. As for isolated monomers, trimers can be photoionized keeping the non-covalent interactions between $H_2O/Na^+/K^+$ and the trimer intact, up to soft X-ray photon energies. The peaks around m/z = 1266, 845 and 634 can be assigned to the intact $(PPG)_{10}$ peptide with two (M^{2+}), three (M^{3+}) and four (M^{4+}) positive charges, respectively. Adducts are also observed, which makes the assignment easier, *e.g.* we can rule out a large contribution of dimers with twice the monomer's charge. Since the initial charges of the peptides within the trimer are most probably two and three, as mentioned earlier, we can assume that detecting the monomer with four charges is due to ionization of a 3+ peptide within the trimer, followed by *inter*-molecular fragmentation (*i.e.* dissociation of the trimer into monomers).

The other peaks can be assigned to *intra*-molecular fragmentation (*i.e.* $(PPG)_{10}$ backbone cleavages). It is interesting that all these fragments also appear in the mass spectra observed with monomers. However, their relative intensities are different: lower for small fragments and higher for large ones. The only exception is a neutral loss (assigned to CO_2) from the precursor ion at 14 eV. Overall, monomer fragmentation is strongly reduced at a given photon energy. All these observations are consistent with complexation effects, due to the substantial increase of the system size (by a factor of three) as well as to the H-bonds between peptides within the trimer. This supports our picture of fragmentation occurring after internal vibrational excitation by photoabsorption. A striking fact is the vanishing of fragmentation around 22 eV: despite the photon energy being at least 8 eV above the ionization energy, the trimer is ionized and remains intact, even without non-covalent bond cleavage (see figure 6).

In figure 6c, relative yields of non-dissociative ionization, inter-molecular fragmentation (sum of monomers) as well as intra-molecular fragmentation (sum of fragments), are plotted as a function of photon energy. After absorption of a single 14 eV photon, the main channel is non-dissociative ionization, but we also observe inter- and intra-molecular fragmentation. When the photon energy rises to 22 eV, the non-dissociative ionization yield increases strongly and reaches a maximum, while inter- and intra-molecular fragmentations *decrease* and reach their minima. This trend is consistent with our observations for isolated monomers (*cf.* figures 3 and 5). Thus, we assign the inter- and intra-molecular fragmentations of the trimer between 14 and 22 eV to photoexcitation without ionization. Interestingly, the yield of intra-molecular fragmentation falls at an energy around 2 eV *lower* than inter-molecular fragmentation. If we assume that photoexcitation deposits some vibrational internal energy into the trimer, which can lead to inter-molecular followed by intra-molecular fragmentation, this is consistent with the average internal energy deposition smoothly *decreasing* with photon energy. This supports our picture proposed for isolated $[(PPG)_{10}+3H]^{3+}$: highly-excited states reached by photoabsorption and smoothly converging to the ground state of the ionized peptide.

For photon energies above 22 eV, non-dissociative ionization decreases while monomers and peptide fragments re-appear smoothly to become the dominant species in the soft X-ray energy range. This suggests that photoabsorption at these energies results in ionized trimers with sufficient internal energy to fragment. Interestingly, the yield of intermolecular fragmentation increases at around 26 eV, whereas the yield of intramolecular fragmentation rises at higher photon energy. Once again, this trend supports the subsequent fragmentation of the monomers emitted from the trimer. The fact that we do not observe peptide fragmentation between 20 and 30 eV is a noticeable difference compared with photoabsorption of isolated monomers, and is likely due to the greater system size and to complexation effects, as said earlier. We recently reported such a size effect for a range of peptides and proteins [12]. For soft X-ray photon energies of 150 and 288 eV, we observe the appearance of peaks in the low m/z range which might be due to a high amount of internal energy deposited in $[((PPG)_{10})_3+7H]^{7+}$. However, at these energies, multiple ionization can also occur [30]. While no evidence of intact multi–ionised species are observed, the presence of internal fragments could also be the result of several radicals created along the peptide backbone by the multi-ionization. As seen in figure 6, single ionization can still be non-dissociative at these energies, showing that, as in the case of isolated $(PPG)_{10}$, a range of orbitals is probed by the photon. The energy of 288 eV corresponds primarily to the excitation of carbon 1s electrons to the π orbital of the peptide bond. This is expected to be followed by Auger decay [38], leading to mainly single but also double ionization, after which the internal energy is typically on the order of 20 eV [12]. Therefore, the energy is ultimately deposited and distributed over the valence band, like for VUV photoabsorption, leading to fragmentation. Moreover, Zagorodskikh *et al.* [39] have shown that acetaldehyde double ionization after single-photon absorption at 40.8 and 95 eV (deep valence shell) is due to simultaneous emission of two electrons. If we assume that the same holds for the collagen mimetic peptides studied here, and since we observe similar spectra for 150 eV and 288 eV, we can conclude that Auger decay does not play a big role in the internal energy deposition and ionization of the collagen $((PPG)_{10})_3$ triple helix model.

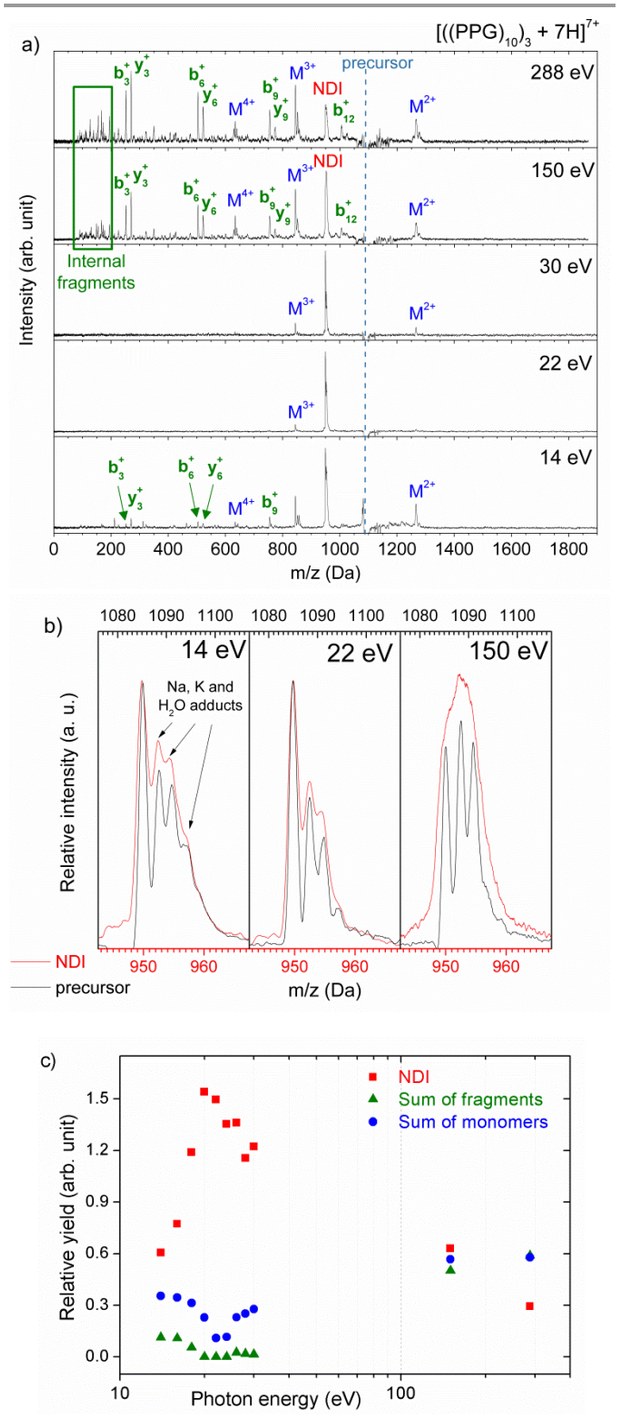

Figure 6 a) Mass spectra of $[((PPG)_{10})_3+7H]^{7+}$ after absorption of one photon of 14, 22, 30, 150 and 288 eV. Peaks corresponding to non-dissociative ionization (NDI), monomers (M) with two, three and four positive charges, and main backbone fragments are spotted. The m/z of the precursor ion is indicated by dashes. b) Superposition of the peaks corresponding to the precursor ion (blue) and non-dissociative single ionization (red) of the triple helix model $[((PPG)_{10})_3+7H]^{7+}$ after photoabsorption of one 14, 22 and 150 eV photon. c) Relative yield of the main channels as a function of the logarithm of photon energy. We summed all monomer charge states to obtain "Sum of monomers" and the singly-charged main backbone fragments for "Sum of fragments".

$((PHypG)_{10})_3$: Effect of Proline Hydroxylation

Photoabsorption experiments on the hydroxylated collagen mimetic peptide trimer with seven charges are presented in figure 7. A mass spectrum after absorption of one 20 eV photon (figure 7a) shows that the dominant channel is non-dissociative photoionization, as for $((PPG)_{10})_3$. We also detect monomers (M^{2+}, M^{3+} and M^{4+}), but a previously unseen species is the dimer (D^{5+}). This is again consistent with the initial presence of one M^{3+} and two M^{2+} monomers in the trimer. The evolution of non-dissociative ionization, monomers and the dimer as a function of photon energy is plotted in figure 7b: the rise of non-dissociative ionization between 14 and 20 eV is the same as in the case of the non-hydroxylated trimer, suggesting that hydroxylation has a negligible effect on the ionization of this species. Above 20 eV, non-dissociative ionization is approximately constant. The high monomer charge states (M^{3+} and M^{4+}) follow the same trend as non-dissociative ionization in the whole energy range, which is in line with inter-molecular fragmentation after photoionization. At 14 eV, the dimer 5+ has about the same yield as the monomer 2+, which is expected if they mainly come from photoexcitation of a trimer 7+ *without ionization*. Then, the dimer yield strongly decreases, while that of the monomer 2+ does much less so. This is probably due to the progressive transition from photoexcitation to photoionization, the latter being followed by dissociation of the trimer into monomers only, which gives a charge distribution of either (2+,3+,3+) or (2+,2+,4+). The fact that the monomer 3+ is more abundant than the 2+ might be due to the higher probability of forming a monomer 3+ compared to a monomer 4+ after single ionization. This could be related to inter-molecular charge transfer before dissociation of the trimer. It is important to note that fragmentation of monomers is not observed at these energies, in sharp contrast with the non-hydroxylated trimer. This is in line with the presence of the dimer after photoexcitation at low energy, and might be linked to a stabilization of the triple helix model by the hydroxyprolines. Previously reported condensed phase experimental work lead to the same conclusion, indicating that this can be explained either by H-bonding between OH groups of hydroxyprolines and H_2O molecules [40], or by stereoelectronic effects tightening the triple helix structure [5]. The fact that our gas phase experiments on the same system also point to a stabilization supports the second hypothesis. It would imply that the triple helix structure is not strongly modified by the electrospray ionization process. Even though native structures have been found to be conserved in the gas phase by this kind of source [41,42], we do not have sound experimental evidence in the case of the collagen mimetic peptide trimers. In the near future, we plan to perform ion mobility spectrometry to measure the collision cross-section of these systems and obtain information about their structure.

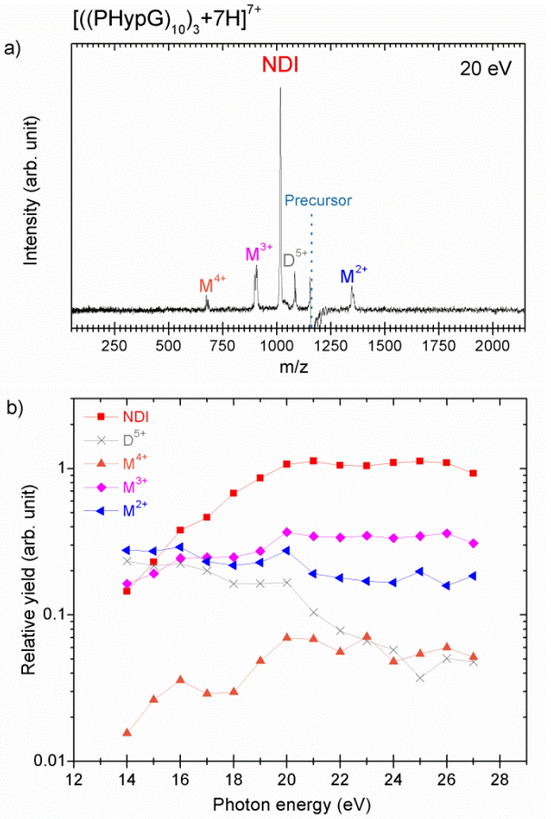

Figure 7 a) Mass spectrum of the collagen mimetic peptide trimer $((PHypG)_{10})_3^{7+}$ after absorption of one 20 eV photon. b) Relative yield of the main channels as a function of photon energy.

Conclusion

We report the first experimental investigation of collagen mimetic peptide photoabsorption in the gas phase using mass spectrometry as a tool to unravel the photo-induced intrinsic molecular processes over a large photon energy range (14-288 eV). At low energy (14-22 eV), our results show that a smooth transition between photoexcitation and photoionization occurs for $(PPG)_{10}$ and $(PHypG)_{10}$ peptides and their trimers. Above 22 eV, photoionization is dominant, and part of the photon energy is converted into a certain amount of molecular vibrational internal energy, which increases with photon energy, leading to more extensive fragmentation. Photoabsorption by the $(PPG)_{10}$ trimer triple helix models first causes inter-molecular fragmentation, then intramolecular fragmentation. The peptidic fragments formed are mainly due to Gly-Pro peptide bond cleavage, in line with previous studies in solution and gas phases, indicating an intrinsically weak site in collagen. The absence of intramolecular fragmentation in the $(PHypG)_{10}$ trimer also show a stabilization of the triple helix structure by hydroxyprolines, probably due to stereoelectronic effects as suggested by solution-phase experiments. More experiments are nevertheless needed to confirm the survival of the triple helix structure in the gas phase for these collagen mimetic peptides.

Acknowledgements

We thank HZB for the allocation of synchrotron radiation beamtime, P. Baumgärtel and T. Kachel for their support during experiments, the European COST action XLIC and the French “Conseil Régional de Normandie” and “Université de Caen Normandie” for funding. The CNRS is acknowledged for a PICS grant (07390) supporting the collaboration between CIMAP/GANIL and the Open University.

Notes and references

1 B. Brodsky and J. A. M. Ramshaw, *Matrix Biol.*, 1997, **15**, 545–554.
2 Y. Li and S. M. Yu, *Curr. Opin. Chem. Biol.*, 2013, **17**, 968–975.
3 A. A. Jalan and J. D. Hartgerink, *Curr. Opin. Chem. Biol.*, 2013, **17**, 960–967.
4 S. Sakakibara, K. Inouye, K. Shudo, Y. Kishida, Y. Kobayashi and D. J. Prockop, *Biochim. Biophys. Acta BBA - Protein Struct.*, 1973, **303**, 198–202.
5 F. W. Kotch, I. A. Guzei and R. T. Raines, *J. Am. Chem. Soc.*, 2008, **130**, 2952.
6 K. Jariashvili, B. Madhan, B. Brodsky, A. Kuchava, L. Namicheishvili and N. Metreveli, *Biopolymers*, 2012, **97**, 189–198.
7 A. Sionkowska, *Int. J. Biol. Macromol.*, 2005, **35**, 145–149.
8 N. Metreveli, L. Namicheishvili, K. Jariashvili, G. Mrevlishvili and A. Sionkowska, *Int. J. Photoenergy*, 2006, 76830.
9 C. A. Miles, A. Sionkowska, S. L. Hulin, T. J. Sims, N. C. Avery and A. J. Bailey, *J. Biol. Chem.*, 2000, **275**, 33014–33020.
10 S. Bari, O. Gonzalez-Magaña, G. Reitsma, J. Werner, S. Schippers, R. Hoekstra and T. Schlathölter, *J. Chem. Phys.*, 2011, **134**, 024314.
11 A. Giuliani, A. R. Milosavljevic, F. Canon and L. Nahon, *Mass Spectrom. Rev.*, 2014, **33**, 424–441.
12 D. Egorov, L. Schwob, M. Lalande, R. Hoekstra and T. Schlatholter, *Phys. Chem. Chem. Phys.*, 2016, **18**, 26213–26223.
13 F. Canon, S. Ployon, J.-P. Mazauric, P. Sarni-Manchado, M. Réfrégiers, A. Giuliani and V. Cheynier, *Chem. Vine Wine Sci.*, 2015, **71**, 3039–3044.
14 F. Canon, A. R. Milosavljević, G. van der Rest, M. Réfrégiers, L. Nahon, P. Sarni-Manchado, V. Cheynier and A. Giuliani, *Angew. Chem. Int. Ed.*, 2013, **52**, 8377–8381.
15 A. R. Milosavljević, V. Z. Cerovski, F. Canon, L. Nahon and A. Giuliani, *Angew. Chem. Int. Ed.*, 2013, **52**, 7286–7290.
16 O. Gonzalez Magana, Doctoral Thesis, University of Groningen, 2013.
17 T. J. D. Jorgensen, D. Delforge, J. Remacle, G. Bojesen and P. Roepstorff, *Int. J. Mass Spectrom.*, 1999, **188**, 63–85.
18 G. D. Chen, R. G. Cooks, D. M. Bunk, M. J. Welch and J. R. Christie, *Int. J. Mass Spectrom.*, 1999, **185**, 75–90.
19 L. Feketeova and R. A. J. O’Hair, *Chem. Commun.*, 2008, 4942–4944.

20 O. González-Magaña, G. Reitsma, M. Tiemens, L. Boschman, R. Hoekstra and T. Schlathölter, *J. Phys. Chem. A*, 2012, **116**, 10745–10751.
21 B. A. Budnik, Y. O. Tsybin, P. Hakansson and R. A. Zubarev, *J. Mass Spectrom.*, 2002, **37**, 1141–1144.
22 L. Schwob, M. Lalande, J. Rangama, D. Egorov, R. Hoekstra, V. Vizcaino, T. Schlathölter and J. C. Poully, to be submitted.
23 J. Berkowitz, *Phys. Essays*, 2000, **13**, 248–255.
24 F. Canon, A. R. Milosavljevic, L. Nahon and A. Giuliani, *Phys. Chem. Chem. Phys.*, 2015, **17**, 25725–25733.
25 Y. M. E. Fung, C. M. Adams and R. A. Zubarev, *J. Am. Chem. Soc.*, 2009, **131**, 9977–9985.
26 A. Giuliani, A. R. Milosavljevic, K. Hinsen, F. Canon, C. Nicolas, M. Refregiers and L. Nahon, *Angew. Chem.-Int. Ed.*, 2012, **51**, 9552–9556.
27 Y. Hatano, *Radiat. Environ. Biophys.*, 1999, **38**, 239–247.
28 O. Plekan, V. Feyer, R. Richter, M. Coreno, M. de Simone, K. C. Prince and V. Carravetta, *J. Phys. Chem. A*, 2007, **111**, 10998–11005.
29 A. P. W. Arachchilage, F. Wang, V. Feyer, O. Plekan and K. C. Prince, *J. Chem. Phys.*, 2010, **133**, 174319.
30 A. R. Milosavljevic, F. Canon, C. Nicolas, C. Miron, L. Nahon and A. Giuliani, *J. Phys. Chem. Lett.*, 2012, **3**, 1191–1196.
31 M. Girod, Z. Sanader, M. Vojkovic, R. Antoine, L. MacAleese, J. Lemoine, V. Bonacic-Koutecky and P. Dugourd, *J. Am. Soc. Mass Spectrom.*, 2015, **26**, 432–443.
32 L. A. Breci, D. L. Tabb, J. R. Yates and V. H. Wysocki, *Anal. Chem.*, 2003, **75**, 1963–1971.
33 C. Bleiholder, S. Suhai, A. G. Harrison and B. Paizs, *J. Am. Soc. Mass Spectrom.*, 2011, **22**, 1032–1039.
34 B. Paizs and S. Suhai, *Mass Spectrom. Rev.*, 2005, **24**, 508–548.
35 A. G. Unnithan, M. J. Myer, C. J. Veale and A. S. Danell, *J. Am. Soc. Mass Spectrom.*, 2007, **18**, 2198–2203.
36 R. N. Grewal, H. El Aribi, A. G. Harrison, K. W. M. Siu and A. C. Hopkinson, *J. Phys. Chem. B*, 2004, **108**, 4899–4908.
37 J. K. Martens, J. Grzetic, G. Berden and J. Oomens, *Int. J. Mass Spectrom.*, 2015, **377**, 179–187.
38 C. Li, P. Salen, V. Yatsyna, L. Schio, R. Feifel, R. Squibb, M. Kaminska, M. Larsson, R. Richter, M. Alagia, S. Stranges, S. Monti, V. Carravetta and V. Zhaunerchyk, *Phys. Chem. Chem. Phys.*, 2016, **18**, 2210–2218.
39 S. Zagorodskikh, V. Zhaunerchyk, M. Mucke, J. H. D. Eland, R. J. Squibb, L. Karlsson, P. Linusson and R. Feifel, *Chem. Phys.*, 2015, **463**, 159–168.
40 J. Bella, B. Brodsky and H. M. Berman, *Struct. Lond. Engl. 1993*, 1995, **3**, 893–906.
41 V. Gabelica, F. Rosu, E. De Pauw, J. Lemaire, J.-C. Gillet, J.-C. Poully, F. Lecomte, G. Gregoire, J.-P. Schermann and C. Desfrancois, *J. Am. Chem. Soc.*, 2008, **130**, 1810–1811.
42 J. C. Poully, G. Grégoire, J. P. Schermann, C. Desfrancois, F. Lecomte, N. Nieuwjaer and B. Manil, *Phys Chem Chem Phys*, 2010, **12**, 3606.